A General Analytical Model for Head Response to Oscillatory Pumping in Unconfined Aquifers: Effects of Delayed Gravity Drainage and Initial Condition

Ching-Sheng Huang[a], Ya-Hsin Tsai[b], Hund-Der Yeh[b*] and Tao Yang[a*]

[a] State Key Laboratory of Hydrology-Water Resources and Hydraulic Engineering, Center for Global Change and Water Cycle, Hohai University, Nanjing 210098, China

[b] Institute of Environmental Engineering, National Chiao Tung University, Hsinchu 300, Taiwan

[*] Corresponding authors:

Hund-Der Yeh; E-mail: hdyeh@mail.nctu.edu.tw; Tel.: +886-3-5731910; fax: +886-3-5725958

Tao Yang; E-mail: tao.yang@hhu.edu.cn; Tel.: +86-13770918075

Submission to *Hydrology and Earth System Sciences* on 11 September 2018

Re-submission to *Hydrology and Earth System Sciences* on 24 December 2018

Key points

1. An analytical model of the hydraulic head due to oscillatory pumping in unconfined aquifers is presented.
2. Head fluctuations affected by instantaneous and delayed gravity drainages are discussed.
3. The effect of initial condition on the phase of head fluctuation is analyzed.
4. The present solution agrees well to head fluctuation data taken from a field oscillatory pumping.

Abstract

Oscillatory pumping tests (OPTs) provide an alternative to constant-head and constant-rate pumping tests for determining aquifer hydraulic parameters when OPT data are analyzed based on an associated analytical model coupled with an optimization approach. There is a large number of analytical models presented for the analysis of OPT. The combined effects of delayed gravity drainage (DGD) and initial condition regarding the hydraulic head are commonly neglected in the existing models. This study aims to develop a new model for describing the hydraulic head fluctuation induced by OPT in an unconfined aquifer. The model contains a groundwater flow equation with the initial condition of static water table, Neumann boundary condition specified at the rim of a partially screened well, and a free surface equation describing water table motion with the DGD effect. The solution is derived using the Laplace, finite-integral, and Weber transforms. Sensitivity analysis is carried out for exploring head response to the change in each of hydraulic parameters. Results suggest the DGD reduces to instantaneous gravity drainage in predicting transient head fluctuation when dimensionless parameter $a_1 = \epsilon S_y b/K_z$ exceeds 500 with empirical constant ϵ, specific yield S_y, aquifer thickness b, and vertical hydraulic conductivity K_z. The water table can be regarded as a no-flow boundary when $a_1 < 10^{-2}$ and $P < 10^4$ s with P being the period of oscillatory pumping rate. A pseudo-steady state model without initial condition causes a time shift from the actual transient model in predicting simple harmonic motion of head fluctuation during a late pumping period. In addition, the present solution agrees well to head fluctuation data observed at the Savannah River site.

KEYWORDS: oscillatory pumping test, analytical solution, free surface equation, delayed gravity drainage, initial condition

45

Notation and Abbreviation

a	$bD_r/(C_y r_w^2)$
a_1, a_2	$b/(\kappa C_y)$, $r_w^2/(\kappa D_r)$
b	Aquifer thickness
C_y	K_z/S_y
D_r	K_r/S_s
DGD	Delayed gravity drainage
h	Hydraulic head
$\bar{h}$	Dimensionless Hydraulic head, i.e., $\bar{h} = 2\pi l K_r h/Q$
IGD	Instantaneous gravity drainage
K_r, K_z	Aquifer horizontal and vertical hydraulic conductivities, respectively
LHS	Left-hand side
l	Screen length, i.e., $z_u - z_l$
OPT	oscillatory pumping test
P	Period of oscillatory pumping rate
PSS	Pseudo-steady state
$\bar{P}$	Dimensionless period, i.e., $\bar{P} = D_r P/r_w^2$
p	Laplace parameter
Q	Amplitude of oscillatory pumping rate
RHS	Right-hand side
r	Radial distance from the center of pumping well
$\bar{r}$	Dimensionless radial distance, i.e., $\bar{r} = r/r_w$
r_w	Radius of pumping well
SHM	Simple harmonic motion
S_s, S_y	Specific storage and specific yield, respectively
t	Time since pumping
$\bar{t}$	Dimensionless pumping time, i.e., $\bar{t} = D_r t/r_w^2$
z	Elevation from aquifer bottom
z_l, z_u	Lower and upper elevations of well screen, respectively
$\bar{z}$	Dimensionless elevation, i.e., $\bar{z} = z/b$
$\bar{z}_l$, $\bar{z}_u$	z_l/b, z_u/b
α	K_z/K_r
β_n	Roots of Eq. (15)
κ	$1/\epsilon$
γ	Dimensionless frequency of oscillatory pumping rate, i.e., $\omega r_w^2/D_r$
ϵ	Empirical constant associated with delayed gravity drainage
μ	$\alpha r_w^2/b^2$
ω	Frequency of oscillatory pumping rate, i.e., $\omega = 2\pi/P$

46

1. Introduction

Numerous attempts have been made by researchers to the study of oscillatory pumping test (OPT) that is an alternative to constant-rate and constant-head pumping tests for determining aquifer hydraulic parameters (e.g., Vine et al., 2016; Christensen et al., 2017; Watlet et al., 2018). The concept of OPT was first proposed by Kuo (1972) in the petroleum literature. The process of OPT contains extraction stages and injection stages. The pumping rate, in other words, varies periodically as a sinusoidal function of time. Compared with traditional constant-rate pumping, OPT in contaminated aquifers has the following advantages: (1) low cost because of no disposing contaminated water from the well, (2) reduced risk of treating contaminated fluid, (3) smaller contaminant movement, and (4) stable signal easily distinguished from background disturbance such as tide effect and varying river stage (e.g., Spane and Mackley, 2011). However, the disadvantages of OPT include the need of an advanced apparatus producing periodic rate. Oscillatory hydraulic tomography adopts several oscillatory pumping wells with different frequencies (e.g., Yeh and Liu, 2000; Cardiff et al., 2013; Zhou et al., 2016; Muthuwatta et al., 2017). Aquifer heterogeneity can be mapped by analyzing multiple data collected from observation wells. Cardiff and Barrash (2011) reviewed articles associated with hydraulic tomography and classified them according to nine categories in a table.

Various groups of researchers have worked with analytical and numerical models for OPT; each group has its own model and investigation. For example, Black and Kipp (1981) assumed the response of confined flow to OPT as simple harmonic motion (SHM) in the absence of initial condition. Cardiff and Barrash (2014) built an optimization formulation strategy using the Black and Kipp analytical solution. Dagan and Rabinovich (2014) also assumed hydraulic head fluctuation as SHM for OPT at a partially screened well in unconfined aquifers. Cardiff et al. (2013) characterized aquifer heterogeneity using the finite element-based COMSOL software that adopts SHM hydraulic head variation for OPT. On the other hand, Rasmussen et al. (2003) found hydraulic head response tends to SHM at a late period of pumping time when

considering initial condition prior to OPT. Bakhos et al. (2014) used the Rasmussen et al. (2003) analytical solution to quantify the time after which hydraulic head fluctuation can be regarded as SHM since OPT began. As mentioned above, most of the models for OPT assume hydraulic head fluctuation as SHM without initial condition, and all of them treat the pumping well as a line source with infinitesimal radius.

Field applications of OPT for determining aquifer parameters have been conducted in recent years. Rasmussen et al. (2003) estimated aquifer hydraulic parameters based on 1- or 2-hour period of OPT at the Savannah River site. Maineult et al. (2008) observed spontaneous potential temporal variation in aquifer diffusivity at a study site in Bochum, Germany. Fokker et al. (2012; 2013) presented spatial distributions of aquifer transmission and storage coefficient derived from curve fitting based on a numerical model and field data from experiments at the southern city-limits of Bochum, Germany. Rabinovich et al. (2015) estimated aquifer parameters of equivalent hydraulic conductivity, specific storage and specific yield at the Boise Hydrogeophysical Research Site by curve fitting based on observation data and the Dagan and Rabinovich (2014) analytical solution. They conclude the equivalent hydraulic parameters can represent the actual aquifer heterogeneity of the study site.

Although a large number of studies have been made in developing analytical models for OPT, little is known about the combined effects of delayed gravity drainage (DGD), finite-radius pumping well, and initial condition prior to OPT. Analytical solution to such a question will not only have important physical implications but also shed light on OPT model development. This study builds an improved model describing hydraulic head fluctuation induced by OPT in an unconfined aquifer. The model is composed of a typical flow equation with the initial condition of static water table, an inner boundary condition specified at the rim of the partially screened well for incorporating finite-radius effect, and a free surface equation describing the motion of water table with the DGD effect. The analytical solution of the model is derived by the methods of Laplace transform, finite-integral transform, and Weber transform.

Based on the present solution, sensitivity analysis is performed to explore the hydraulic head in response to the change in each of hydraulic parameters. The effects of DGD and instantaneous gravity drainage (IGD) on the head fluctuations are compared. The quantitative criterion for treating the well radius as infinitesimal is discussed. The effect of the initial condition on the phase of head fluctuation is investigated. In addition, curve fitting of the present solution to head fluctuation data recorded at the Savannah River site is presented.

2. Methodology

2.1. Mathematical model

Consider an OPT in an unconfined aquifer illustrated in Fig. 1. The aquifer is of unbound lateral extent with a finite thickness b. The radial distance from the centerline of the well is r; an elevation from the impermeable bottom of the aquifer is z. The well with outer radius r_w is screened from elevation z_u to z_l.

The flow equation describing spatiotemporal head distribution in aquifers can be written as:

$$D_r\left(\frac{\partial^2 h}{\partial r^2}+\frac{1}{r}\frac{\partial h}{\partial r}+\alpha\frac{\partial^2 h}{\partial z^2}\right)=\frac{\partial h}{\partial t} \quad \text{for} \quad r_w \le r < \infty,\ 0 \le z \le b \quad \text{and} \quad t \ge 0 \qquad (1)$$

where $D_r = K_r/S_s$; $\alpha = K_z/K_r$; $h(r,z,t)$ is hydraulic head at location (r, z) and time t; K_r and K_z are respectively the radial and vertical hydraulic conductivities; S_s is the specific storage. Consider water table as a reference datum where the elevation head is set to zero; the initial condition is expressed as:

$$h = 0 \ \text{at} \ t = 0 \qquad (1)$$

The rim of the wellbore is regarded as an inner boundary under the Neumann condition expressed as:

$$2\pi r_w K_r l\frac{\partial h}{\partial r} = \begin{cases} Q\sin(\omega t) & \text{for} \quad z_l \le z \le z_u \\ 0 & \text{outside screen interval} \end{cases} \quad \text{at} \quad r{=}r_w \qquad (2)$$

where $l = z_u - z_l$ is screen length; Q and $\omega = 2\pi/P$ are respectively the amplitude and frequency of oscillatory pumping rate (i.e., $Q\sin(\omega t)$) with a period P. Water table motion can

be defined by Eq. (4a) for IGD (Neuman, 1972) and Eq. (4b) for DGD (Moench, 1995).

$$\frac{\partial h}{\partial z} = -\frac{1}{C_y}\frac{\partial h}{\partial t} \quad \text{at} \quad z = b \ \text{ for IGD} \tag{3a}$$

$$\frac{\partial h}{\partial z} = \frac{1}{\kappa C_y}\int_0^t \frac{\partial h}{\partial \tau}\exp(-(t-\tau)/\kappa)\,d\tau \quad \text{at} \quad z = b \ \text{ for DGD} \tag{4b}$$

where $C_y = K_z/S_y$, $\kappa = 1/\epsilon$ with ϵ being an empirical constant, and S_y is the specific yield. Note that Eq. (4b) reduces to Eq. (4a) when $\kappa \to \infty$ or $\epsilon = 0$. The impervious aquifer bottom is under the no-flow condition:

$$\frac{\partial h}{\partial z} = 0 \quad \text{at} \quad z = 0 \tag{4}$$

The hydraulic head far away from the pumping well remains constant, written as

$$\lim_{r\to\infty} h(r,z,t) = 0 \tag{5}$$

Define dimensionless variables and parameters as follows:

$$\bar{h} = \frac{2\pi l K_r}{Q}h,\ \bar{r} = \frac{r}{r_w},\ \bar{z} = \frac{z}{b},\ \bar{z}_l = \frac{z_l}{b},\ \bar{z}_u = \frac{z_u}{b},\ \bar{t} = \frac{D_r}{r_w^2}t,\ \bar{\tau} = \frac{D_r}{r_w^2}\tau,\ \bar{P} = \frac{D_r}{r_w^2}P$$

$$\gamma = \frac{\omega r_w^2}{D_r},\ \mu = \frac{\alpha r_w^2}{b^2}, a = \frac{bD_r}{C_y r_w^2},\ a_1 = \frac{b}{\kappa C_y},\ a_2 = \frac{r_w^2}{\kappa D_r} \tag{6}$$

where the overbar stands for a dimensionless symbol. Note that the magnitude of a_1 is related to the DGD effect (Moench, 1995) and γ is a dimensionless frequency parameter. With Eq. (7), the dimensionless forms of Eqs. (1) - (6) become, respectively,

$$\frac{\partial^2 \bar{h}}{\partial \bar{r}^2} + \frac{1}{\bar{r}}\frac{\partial \bar{h}}{\partial \bar{r}} + \mu\frac{\partial^2 \bar{h}}{\partial \bar{z}^2} = \frac{\partial \bar{h}}{\partial \bar{t}} \quad \text{for} \quad 1 \le \bar{r} < \infty,\ 0 \le \bar{z} < 1 \quad \text{and} \quad \bar{t} \ge 0 \tag{7}$$

$$\bar{h} = 0 \quad \text{at} \quad \bar{t} = 0 \tag{8}$$

$$\frac{\partial \bar{h}}{\partial \bar{r}} = \begin{cases} \sin(\gamma \bar{t}) & \text{for} \quad \bar{z}_l \le \bar{z} \le \bar{z}_u \\ 0 & \text{outside screen interval} \end{cases} \quad \text{at} \quad \bar{r} = 1 \tag{9}$$

$$\frac{\partial \bar{h}}{\partial \bar{z}} = -a\frac{\partial \bar{h}}{\partial \bar{t}} \quad \text{at} \quad \bar{z} = 1 \ \text{ for IGD} \tag{10a}$$

$$\frac{\partial \bar{h}}{\partial \bar{z}} = -a_1\int_0^{\bar{t}} \frac{\partial \bar{h}}{\partial \bar{\tau}}\exp(-a_2(\bar{t}-\bar{\tau}))\,d\bar{\tau} \quad \text{at} \quad \bar{z} = 1 \ \text{ for DGD} \tag{11b}$$

$$\frac{\partial \bar{h}}{\partial \bar{z}} = 0 \quad \text{at} \quad \bar{z} = 0 \tag{12}$$

$$\lim_{\bar{r}\to\infty} \bar{h}(\bar{r},\bar{z},\bar{t}) = 0 \tag{13}$$

Eqs. (8) – (13) represent the transient DGD model when excluding (11a) and transient IGD model when excluding (11b).

2.2. Transient solution for unconfined aquifer

The Laplace transform and finite-integral transform are applied to solve Eqs. (8) - (13) (Latinopoulos, 1985; Liang et al., 2017; 2018). The transient solution can then be expressed as

$$\bar{h}(\bar{r},\bar{z},\bar{t}) = \bar{h}_{\text{exp}}(\bar{r},\bar{z},\bar{t}) + \bar{h}_{\text{SHM}}(\bar{r},\bar{z},\bar{t}) \quad (14a)$$

with

$$\bar{h}_{\text{exp}}(\bar{r},\bar{z},\bar{t}) = \frac{-2\gamma}{\pi}\sum_{n=1}^{\infty}\int_0^{\infty}\cos(\beta_n\bar{z})\exp(p_0\bar{t})\,\text{Im}(\varepsilon_1\varepsilon_2)\;\;d\zeta \quad (14b)$$

$$\bar{h}_{\text{SHM}}(\bar{r},\bar{z},\bar{t}) = \bar{A}_t(\bar{r},\bar{z})\cos\big(\gamma\bar{t} - \phi_t(\bar{r},\bar{z})\big) \quad (14c)$$

$$\bar{A}_t(\bar{r},\bar{z}) = \sqrt{a_t(\bar{r},\bar{z})^2 + b_t(\bar{r},\bar{z})^2} \quad (14d)$$

$$a_t(\bar{r},\bar{z}) = \frac{2}{\pi}\sum_{n=1}^{\infty}\int_0^{\infty} p_0\cos(\beta_n\bar{z})\,\text{Im}(\varepsilon_1\varepsilon_2)\,d\zeta \quad (14e)$$

$$b_t(\bar{r},\bar{z}) = \frac{2\gamma}{\pi}\sum_{n=1}^{\infty}\int_0^{\infty}\cos(\beta_n\bar{z})\,\text{Im}(\varepsilon_1\varepsilon_2)\,d\zeta \quad (14f)$$

$$\phi_t(\bar{r},\bar{z}) = \cos^{-1}\big(b_t(\bar{r},\bar{z})/\bar{A}_t(r,\bar{z})\big) \quad (14g)$$

$$\varepsilon_1 = K_0(\lambda_0\bar{r})(\sin(\bar{z}_u\beta_n) - \sin(\bar{z}_l\beta_n))/(\beta_n\lambda_0 K_1(\lambda_0)(p_0^2+\gamma^2)) \quad (14h)$$

$$\varepsilon_2 = (\beta_n^2 + c_0^2)/(\beta_n^2 + c_0^2 + c_0) \quad (14i)$$

$$p_0 = -\zeta - \mu\beta_n^2 \quad (14j)$$

$$\lambda_0 = \sqrt{\zeta}\,i \quad (14k)$$

where $c_0 = ap_0$ for IGD and $a_1p_0/(p_0+a_2)$ for DGD, i is the imaginary unit, Im(-) is the imaginary part of a complex number, $K_0(-)$ and $K_1(-)$ are the modified Bessel functions of the second kind of order zero and one, respectively, and β_n is the positive roots of the equation:

$$\tan\beta_n = c_0/\beta_n \quad (15)$$

The method to find the roots of β_n is discussed in Section 2.3. The detailed derivation of Eqs. (14a) – (14k) is presented in the supporting material. The first term on the right-hand side (RHS) of Eq. (14a) exhibits exponential decay due to the initial condition since pumping began;

the second term defines SHM with amplitude $\bar{A}_t(\bar{r},\bar{z})$ and phase shift $\phi_t(\bar{r},\bar{z})$ at a given point $(\bar{r},\bar{z})$. The numerical results of the integrals in Eqs. (14b), (14e) and (14f) are obtained by the Mathematica NIntegrate function.

2.3. Calculation of β_n

The eigenvalues β_1, …, β_n, the roots of Eq. (15) can be determined by applying the Mathematica function FindRoot based on Newton's method with reasonable initial guesses. The roots are located at the intersection of the curves plotted by the RHS and left-hand side (LHS) functions of β_n in Eq. (15). The roots are very close to the vertical asymptotes of the periodical tangent function $\tan\beta_n$. When $c_0 = ap_0$, the initial guess for each β_n can be considered as $\beta_{0,n} + \delta$ where $\beta_{0,n} = (2n-1)\pi/2$, $n \in (1,2,\ldots\infty)$ and δ is a small positive value set to 10^{-10}. When $c_0 = a_1p_0/(p_0+a_2)$, the initial guess is set to $\beta_{0,n} - \delta$ for $a_2 - \zeta \le 0$. There is an additional vertical asymptote at $\beta_n = \sqrt{(a_2 - \zeta)/\mu}$ derived from the RHS function of Eq. (15) (i.e., $p_0 + a_2 = 0$) if $a_2 - \zeta > 0$. The initial guess is therefore set to $\beta_{0,n} + \delta$ for $\beta_{0,n}$ on the LHS of the asymptote and $\beta_{0,n} - \delta$ for $\beta_{0,n}$ on the RHS.

2.4. Transient solution for confined aquifer

When S_y = 0 (i.e., $a = 0$ or $a_1 = 0$), Eq. (11a) or (11b) reduces to $\partial\bar{h}/\partial\bar{z} = 0$ for no-flow condition at the top of the aquifer, indicating the unconfined aquifer becomes a confined one. Under this condition, Eq. (15) becomes $\tan\beta_n = 0$ with roots $\beta_n = 0,\ \pi,\ 2\pi,\ \ldots,\ n\pi,\ \ldots,\ \infty$; Eq. (14i) reduces to $\varepsilon_2 = 1$; factor 2 in Eqs. (14b), (14e) and (14f) is replaced by unity for $\beta_n = 0$ and remains for the others. The analytical solution of the transient head for the confined aquifer can be expressed as Eqs. (14a) - (14k) with

$$\bar{h}_{\exp}(\bar{r},\bar{z},\bar{t}) = \frac{-\gamma}{\pi}\int_0^\infty \mathrm{Im}(\varepsilon_0)\exp(-\zeta\bar{t})\,d\zeta - \frac{2\gamma}{\pi}\sum_{n=1}^{\infty}\int_0^\infty \cos(n\pi\bar{z})\,\mathrm{Im}(\varepsilon_1)\exp(p_0\bar{t})\,d\zeta \tag{16a}$$

$$a_t(\bar{r},\bar{z}) = -\frac{1}{\pi}\int_0^\infty \zeta\,\mathrm{Im}(\varepsilon_0)\,d\zeta + \frac{2}{\pi}\sum_{n=1}^{\infty}\int_0^\infty p_0\cos(n\pi\bar{z})\,\mathrm{Im}(\varepsilon_1)\,d\zeta \tag{16b}$$

$$b_t(\bar{r},\bar{z}) = \frac{\gamma}{\pi}\int_0^\infty \mathrm{Im}(\varepsilon_0)\,d\zeta + \frac{2\gamma}{\pi}\sum_{n=1}^\infty \int_0^\infty \cos(n\pi\bar{z})\,\mathrm{Im}(\varepsilon_1)\,d\zeta \quad (16c)$$

$$\varepsilon_0 = (\bar{z}_u - \bar{z}_l)K_0(\lambda_0\bar{r})/(\lambda_0 K_1(\lambda_0)(\zeta^2+\gamma^2)) \quad (16d)$$

Note that Eq. (14h) reduces to Eq. (16d) based on $\beta_n = 0$ and L' Hospital's rule. When $\bar{z}_u = 1$ and $\bar{z}_l = 0$ for the case of full screen, Eq. (14h) gives $\varepsilon_1 = 0$ for $\beta_n > 0$ and the second RHS terms of Eqs. (16a) – (16c) can therefore be eliminated. This causes the solution for confined aquifers is independent of dimensionless elevation $\bar{z}$, indicating only horizontal flow in the aquifer.

2.5. Pseudo-steady state solution for unconfined aquifer

A pseudo-steady state (PSS) solution $\bar{h}_s$ accounts for SHM of head fluctuation at a late period of pumping time and satisfies the following form (Dagan and Rabinovich, 2014)

$$\bar{h}_s(\bar{r},\bar{z},\bar{t}) = \mathrm{Im}\left(\bar{H}(\bar{r},\bar{z})\ e^{i\gamma\bar{t}}\right) \quad (17)$$

where $\bar{H}(\bar{r},\bar{z})$ is a space function of $\bar{r}$ and $\bar{z}$. Define a PSS IGD model as Eqs. (8) - (13) excluding (9), (11b) and replacing $\sin(\gamma\bar{t})$ in (10) by $e^{i\gamma\bar{t}}$. Substituting Eq. (17) and $\partial\bar{h}_s/\partial\bar{t} = \mathrm{Im}\left(i\gamma\bar{H}(\bar{r},\bar{z})\ e^{i\gamma\bar{t}}\right)$ into the model results in

$$\frac{\partial^2\bar{H}}{\partial\bar{r}^2} + \frac{1}{\bar{r}}\frac{\partial\bar{H}}{\partial\bar{r}} + \mu\frac{\partial^2\bar{H}}{\partial\bar{z}^2} = i\gamma\bar{H} \quad (18)$$

$$\frac{\partial\bar{H}}{\partial\bar{r}} = \begin{cases} 1 & \text{for } \bar{z}_l \le \bar{z} \le \bar{z}_u \\ 0 & \text{outside screen interval} \end{cases} \quad \text{at } \bar{r} = 1 \quad (19)$$

$$\frac{\partial\bar{H}}{\partial\bar{z}} = -ia\gamma\bar{H} \quad \text{at} \quad \bar{z} = 1 \text{ for IGD} \quad (20)$$

$$\frac{\partial\bar{H}}{\partial\bar{z}} = 0 \quad \text{at} \quad \bar{z} = 0 \quad (21)$$

$$\lim_{\bar{r}\to\infty}\bar{H} = 0 \quad (22)$$

The resultant model is independent of $\bar{t}$, indicating the analytical solution of $\bar{H}(\bar{r},\bar{z})$ is tractable. Similarly, consider a PSS DGD model that equals the PSS IGD model but replaces (11a) by (11b). Substituting Eq. (17) into the result yields a model that depends on $\bar{t}$, indicating the solution $\bar{h}_s$ to the PSS DGD model is not tractable.

The Weber transform, defined in Eq. (B.1) of the supporting material, may be considered

as a Hankel transform with a more general kernel function. It can be applied to diffusion-type problems with a radial-symmetric region from a finite distance to infinity. For groundwater flow problems, it can be used to develop the analytical solution for the flow equation with a Neumann boundary condition specified at the rim of a finite-radius well (e.g., Lin and Yeh, 2017; Povstenko, 2015). Taking the transform and the formula of $e^{i\gamma\bar{t}} = \cos(\gamma\bar{t}) + i\sin(\gamma\bar{t})$ to solve Eqs. (18) - (22) yields the solution of $\bar{h}_s$ expressed as

$$\bar{h}_s(\bar{r},\bar{z},\bar{t}) = \bar{A}_s(\bar{r},\bar{z})\cos\big(\gamma t - \phi_s(\bar{r},\bar{z})\big) \tag{23a}$$

$$\bar{A}_s(\bar{r},\bar{z}) = \sqrt{a_s(\bar{r},\bar{z})^2 + b_s(\bar{r},\bar{z})^2} \tag{23b}$$

$$a_s(\bar{r},\bar{z}) = \mathrm{Re}\big(\bar{H}(\bar{r},\bar{z})\big) \tag{23c}$$

$$b_s(\bar{r},\bar{z}) = \mathrm{Im}\big(\bar{H}(\bar{r},\bar{z})\big) \tag{23d}$$

$$\phi_s(\bar{r},\bar{z}) = \cos^{-1}\big(b_s(\bar{r},\bar{z})/A_s(\bar{r},\bar{z})\big) \tag{23e}$$

$$\bar{H}(\bar{r},\bar{z}) = \begin{cases} \int_0^\infty \widetilde{H}_u \ \xi \ \Omega \ d\xi & \text{for} \quad \bar{z}_u < \bar{z} \le 1 \\ \int_0^\infty \widetilde{H}_m \ \xi \ \Omega \ d\xi & \text{for} \quad \bar{z}_l \le \bar{z} \le \bar{z}_u \\ \int_0^\infty \widetilde{H}_l \ \xi \ \Omega \ d\xi & \text{for} \quad 0 \le \bar{z} < \bar{z}_l \end{cases} \tag{23f}$$

$$\Omega = \big(J_0(\xi\bar{r})Y_1(\xi) - Y_0(\xi\bar{r})J_1(\xi)\big)/\big(J_1^2(\xi) + Y_1^2(\xi)\big) \tag{23g}$$

with the Bessel functions of the first kind of order zero $J_0(-)$ and one $J_1(-)$ as well as the second kind of order zero $Y_0(-)$ and one $Y_1(-)$,

$$\begin{cases} \widetilde{H}_u = \widetilde{H}_p(c_1\exp(\lambda_w\bar{z}) + c_2\exp(-\lambda_w\bar{z})) & \text{for} \quad \bar{z}_u < \bar{z} \le 1 \\ \widetilde{H}_m = \widetilde{H}_p(c_3\exp(\lambda_w\bar{z}) + c_4\exp(-\lambda_w\bar{z}) - 1) & \text{for} \quad \bar{z}_l \le \bar{z} \le \bar{z}_u \\ \widetilde{H}_l = \widetilde{H}_p c_5(\exp(\lambda_w\bar{z}) + \exp(-\lambda_w\bar{z})) & \text{for} \quad 0 \le \bar{z} < \bar{z}_l \end{cases} \tag{23h}$$

$$c_1 = -e^{-\lambda_w}(\lambda_w - \sigma)(\sinh(\bar{z}_l\lambda_w) - \sinh(\bar{z}_u\lambda_w))/D \tag{23i}$$

$$c_2 = -e^{\lambda_w}(\lambda_w + \sigma)(\sinh(\bar{z}_l\lambda_w) - \sinh(\bar{z}_u\lambda_w))/D \tag{23j}$$

$$c_3 = \frac{e^{-(1+\bar{z}_l+\bar{z}_u)\lambda_w}}{2D}\Big(\sigma\big(e^{(2+\bar{z}_l)\lambda_w} + e^{\bar{z}_u\lambda_w} - e^{(2\bar{z}_l+\bar{z}_u)\lambda_w}\big) + (\sigma - \lambda_w)e^{(\bar{z}_l+2\bar{z}_u)\lambda_w} + \lambda_w\big(e^{(2+\bar{z}_l)\lambda_w} - e^{\bar{z}_u\lambda_w} + e^{(2\bar{z}_l+\bar{z}_u)\lambda_w}\big)\Big) \tag{23k}$$

$$c_4 = \frac{e^{-(1+\bar{z}_l+\bar{z}_u)\lambda_w}}{2D}\Big((\sigma - \lambda_w)e^{(\bar{z}_l+2\bar{z}_u)\lambda_w} + (\sigma + \lambda_w)(e^{(2+\bar{z}_l)\lambda_w} - e^{(2+\bar{z}_u)\lambda_w} +$$

$e^{(2+2\bar{z}_l+\bar{z}_u)\lambda_w}\big)\big)$ (23l)

$c_5 = \frac{1}{2D} e^{-(1+\bar{z}_l+\bar{z}_u)\lambda_w}(e^{\bar{z}_l\lambda_w} - e^{\bar{z}_u\lambda_w})((\lambda_w - \sigma)e^{(\bar{z}_l+\bar{z}_u)\lambda_w} + (\lambda_w + \sigma)e^{2\lambda_w})$ (23m)

where $\lambda_w^2 = (\xi^2 + i\gamma)/\mu$, $\sigma = i\gamma a$, $\tilde{H}_p = 2/(\pi\mu\xi\lambda_w^2)$ and $D = 2(\sigma\cosh\lambda_w + \lambda_w \sinh\lambda_w)$, and Re(-) is the real part of a complex number. Again, one can refer to the supporting material for the derivation of the solution. Eq. (23a) indicates SHM for the response of the hydraulic head at any point to oscillatory pumping. Note that Eq. (23f) reduces to $\bar{H}(\bar{r},\bar{z}) = \int_0^\infty \tilde{H}_m \ \xi \ \Omega \ d\xi$ for a fully screened well when $\bar{z}_l = 0$ and $\bar{z}_u = 1$.

2.6. Pseudo-steady state solution for confined aquifers

Applying the finite Fourier cosine transform to the model, Eqs. (18) – (22) with $S_y = 0$ (i.e., $a = 0$) for the confined condition, leads to an ordinary differential equation with two boundary conditions. With solving the boundary-value problem, the solution of $\bar{h}_s$ for confined aquifers can be expressed as Eqs. (23a) - (23e) with $\bar{H}(\bar{r},\bar{z})$ defined as

$$\bar{H}(\bar{r},\bar{z}) = -2\sum_{m=0}^{\infty} \frac{K_0(\bar{r}\lambda_m)}{\lambda_m K_1(\lambda_m)} \times \begin{cases} 0.5(\bar{z}_u - \bar{z}_l) & \text{for} \quad m = 0 \\ \frac{\cos(m\pi\bar{z})}{m\pi}(\sin(\bar{z}_u m\pi) - \sin(\bar{z}_l m\pi)) & \text{for} \quad m > 0 \end{cases} \quad (24)$$

where $\lambda_m^2 = \gamma i + \mu(m\pi)^2$. The derivation of Eq. (24) is also listed in the supporting material. For a fully screened well (i.e., $\bar{z}_u = 1$, $\bar{z}_l = 0$), the first term of the series (i.e., $m = 0$) remains and the others equal zero because of $\sin(\bar{z}_u m\pi) - \sin(\bar{z}_l m\pi) = 0$. The result is independent of dimensionless elevation $\bar{z}$, indicating the confined flow is only horizontal.

2.7. Special cases of the present solution

Table 1 classifies the present solution (i.e., Solution 1) and its special cases (i.e., Solutions 2 to 6) according to transient or PSS flow, unconfined or confined aquifer, and IGD or DGD. Each of Solutions 1 to 6 reduces to a special case for fully screened well. Existing analytical solutions can be regarded as special cases of the present solution as discussed in Section 3.4 (e.g., Black and Kipp, 1981; Rasmussen et al., 2003; Dagan and Rabinovich, 2014).

2.8. Sensitivity analysis

Sensitivity analysis evaluates hydraulic head variation in response to the change in each of K_r, K_z, S_s, S_y, ω, and ε. The normalized sensitivity coefficient can be defined as (Liou and Yeh, 1997)

$$S_i = P_i \frac{\partial X}{\partial P_i} \tag{25}$$

where S_i is the sensitivity coefficient of ith parameter; P_i is the magnitude of the ith input parameter; X represents the present solution in dimensional form. Eq. (25) can be approximated as

$$S_i = P_i \frac{X(P_i+\Delta P_i)-X(P_i)}{\Delta P_i} \tag{26}$$

where ΔP_i, a small increment, is chosen as $10^{-3}P_i$.

3. Results and Discussion

The following sections demonstrate the response of the hydraulic head to oscillatory pumping using the present solution. The default values in calculation are r = 0.05 m, z = 5 m, b = 10 m, $Q = 10^{-3}$ m^3/s, r_w = 0.05 m, z_u = 5.5 m, z_l = 4.5 m, $K_r = 10^{-4}$ m/s, $K_z = 10^{-5}$ m/s, $S_s = 10^{-5}$ m^{-1}, $S_y = 10^{-4}$, $\omega = 2\pi/30$ s^{-1}, and $\kappa = 100$ s. The corresponding dimensionless parameters and variables are $\bar{r} = 1$, $\bar{z} = 0.5$, $\bar{z}_u = 0.55$, $\bar{z}_l = 0.45$, $\gamma = 5.24\times10^{-5}$, $\mu = 2.5 \times 10^{-6}$, $a = 4 \times 10^5$, $a_1 = 1$ and $a_2 = 2.5 \times 10^{-6}$.

3.1. Delayed gravity drainage

Previous analytical models for OPT consider either confined flow (e.g., Rasmussen et al., 2003) or unconfined flow with IGD effect (e.g., Dagan and Rabinovich, 2014). Little attention has been paid to the consideration of the DGD effect. This section addresses the diffrence among these three models. Figure 2 shows the curve of the dimensionless amplitude $\bar{A}_t$ at ($\bar{r}$, $\bar{z}$) = (1, 1) of Solution 1 versus the dimensionless parameter a_1 related to the DGD effect. The transient head fluctuations are plotted based on Solution 1 with $a_1 = 10^{-2}$, 1, 10, 500, Solution 2 for IGD and Solution 3 for confined flow. Define the relative error as

$$RE = |\bar{A}_t' - \bar{A}_t|/\bar{A}_t \tag{27}$$

where $\bar{A}_t'$ is the dimensionless amplitude predicted by Solution 2 for the case of $a_1 = 500$ or Solution 3 for the case of $a_1 = 10^{-2}$. The curves of the *RE* versus the period of oscillatory pumping rate (i.e., *P*) for these two cases are displayed. The range of $P \leq 10^5$s (1.16 d) contains most practical applications of OPT. When $10^{-2} \leq a_1 \leq 500$, the $\bar{A}_t$ gradually decreases with a_1 to the trough and then increases to the ultimate value of $\bar{A}_t = 1.79 \times 10^{-2}$. The DGD, in other words, causes an effect. When $a_1 < 10^{-2}$, Solutions 1 and 3 agree on the predicted heads; the *RE* is below 1% for $P < 10^4$s (2.78 h), indicating the unconfined aquifer with the DGD effect behaves like confined aquifer and the water table can be regarded as a no-flow boundary when $a_1 < 10^{-2}$ and $P < 10^4$s. When $a_1 > 500$, the head fluctuations predicted by both Solutions 1 and 2 are identical; the largest *RE* is about 0.45%, indicating the DGD effect is ignorable and Eq. (4b) reduces to (4a) for the IGD condition. This conclusion is applicable for any magnitude of *P* in spite of $P > 10^5$s.

3.2. Effect of finite radius of pumping well

Existing analytical models for OPT mostly treated the pumping well as a line source with infinitesimal radius (e.g., Rasmussen et al., 2003; Dagan and Rabinovich, 2014). The finite difference scheme for the model also treats the well as a nodal point by neglecting the radius. These will lead to significant error when a well has the radius ranging from 0.5 m to 2 m (Yeh and Chang, 2013). This section discusses the relative error in predicted amplitude defined as

$$RE = |\bar{A}_{D\&R} - \bar{A}_t|/\bar{A}_t \quad (28)$$

where $\bar{A}_t$ and $\bar{A}_{D\&R}$ are the dimensionless amplitudes at $\bar{r} = 1$ (i.e., $r = r_w$) predicted by IGD Solution 2 and the Dagan and Rabinovich (2014) solution, respectively. Note that their solution assumes infinitesimal radius of a pumping well and has a typo that the term $e^{-D_w+1} - e^{-D_w}$ should read $e^{\beta(-D_w+1)} - e^{-\beta D_w}$ (see their Eq. (25)). Figure 3 demonstrates the *RE* for different values of radius r_w. The RE increases with r_w as expected. For case 1 of r_w = 0.1 m, both solutions agree well in the entire domain of $1 \leq \bar{r} \leq \infty$, indicating a pumping well with $r_w \leq$ 0.1 m can be regarded as a line source. For the extreme case 2 of r_w = 1 m or case 3 of

315 r_w = 2 m, the Dagan and Rabinovich solution underestimates the dimensionless amplitude for
316 $1 \le \bar{r} \le 6$ and agrees to the present solution for $\bar{r} > 6$. The *RE*s for these two cases exceed
317 10%. The effect of finite radius should therefore be considered in OPT models especially when
318 observed hydrulic head data are taken close to the wellbore of a large-diameter well.

319 **3.3. Sensitivity analysis**

320 The temporal distributions of normalized sensitivity coefficient S_i defined as Eq. (26) with
321 $X = h_{\exp}$ of Solution 1 are displayed in Fig. 4a for the response of exponential decay to the
322 change in each of six parameters K_r, K_z, S_s, S_y, ω and ε. The exponential decay is very sensitive
323 to variation in each of K_r, K_z, S_s and ω because of $|S_i| > 0$. Precisely, a positive perturbation
324 in S_s produces an increase in the magnitude of $h_{\exp}$ while that in K_r or K_z causes a decrease.
325 In addition, a positive perturbation in ω yields an increase in $h_{\exp}$ before t = 1 s and a decrease
326 after that time. It is worth noting that S_i for S_y or ε is very close to zero over the entire period
327 of time, indicating $h_{\exp}$ is insensitive to the change in S_y or ε and the subtle change of gravity
328 drainage has no influence on the exponential decay. On the other hand, the spatial distributions
329 of S_i associated with the amplitude A_t are shown in Fig. 4b in response to the changes in
330 those six parameters. The A_t is again sensitive to the change in each of K_r, K_z, S_s and ω but
331 insensitive with the change in S_y or ε. The same result of $|S_i| \cong 0$ for S_y or ε applies to any
332 observation point under the water table (i.e., $\bar{z} < 1$), but $|S_i| > 0$ at the water table (i.e., $\bar{z} =$
333 1) shown in Fig. 4c. From those discussed above, we may conclude the changes in the four key
334 parameters K_r, K_z, S_s and ω significantly affect head prediction in the entire aquifer domain.
335 The change in S_y or ε leads to insignificant variation in the predicted head below the water
336 table and slight variation at the water table.

337 **3.4. Transient head fluctuation affected by the initial condition**

338 Figure 5 demonstrates head fluctuations predicted by DGD Solution 1 and IGD Solution 2
339 expressed as $\bar{h} = \bar{h}_{\exp} + \bar{h}_{\mathrm{SHM}}$ for transient flow and by IGD solution as $\bar{h}_s = \bar{A}_s \cos(\gamma t -$
340 $\phi_s)$ for PSS flow. The transient head fluctuation starts from $\bar{h}$ = 0 at $\bar{t}$ = 0 and approaches

SHM predicted by $\bar{h}_{\mathrm{SHM}}$ when $\bar{h}_{\mathrm{exp}} \cong 0$ m after $\bar{t} = 0.5\bar{P}$ (i.e., 6×10^4). Solutions 1 and 2 agree to the $\bar{h}$ predictions because the head at $\bar{z} = 0.5$ under the water table is insensitive to the change in S_y or ε as discussed in Section 3.3. It is worth noting that the solution of Dagan and Rabinovich (2014) for PSS flow has a time shift from the $\bar{h}_{\mathrm{SHM}}$ of Solution 2. This indicates the phase of their solution (i.e., 1.50 rad) should be replaced by the phase of Solution 2 (i.e., $\phi_t = 1.64$ rad) so that their solution exactly fits the $\bar{h}_{\mathrm{SHM}}$ of Solution 2.

Figure 6 displays head fluctuations predicted by transient Solution 3 expressed as $\bar{h} = \bar{h}_{\mathrm{exp}} + \bar{h}_{\mathrm{SHM}}$ and PSS Solution 6 as $\bar{h}_s = \bar{A}_s \cos(\gamma t - \phi_s)$ for partially screened pumping well in panel (a) and full screen in panel (b). The Rasmussen et al. (2003) solution for transient flow predicts the same $\bar{h}$ as Solution 3. The Black and Kipp (1981) for PPS flow also predicts close $\bar{h}_{\mathrm{SHM}}$ prediction of Solution 3. The phase of Solution 6 (i.e., ϕ_s = 1.50 rad for panel (a) and 1.33 rad for (b)) can be replaced by the phase of Solution 3 (i.e., $\phi_t = 1.64$ rad for (a) and 1.81 rad for (b)) so that the $\bar{h}_{\mathrm{SHM}}$ prediction of Solutions 3 is identical to the $\bar{h}_s$ prediction of Solution 6. As concluded, excluding the initial condition with Eq. (17) for a PSS model leads to a time shift from the SHM of the head fluctuation predicted by the associated transient model while the transient and PSS models give the same SHM amplitude.

3.5. Application of the present solution to field experiment

Rasmussen et al. (2003) conducted field OPTs in a three-layered aquifer system containing one Surficial Aquifer, the Barnwell-McBean Aquifer in between and the deepest Gordon Aquifer at the Savannah River site. Two clay layers dividing these three aquifers may be regarded as impervious strata. For the OPT at the Surficial Aquifer, the formation has 6.25 m averaged thickness near the test site. The fully-screened pumping well has 7.6 cm outer radius. The pumping rate can be approximated as $Q\sin(\omega t)$ with $Q = 4.16\times10^{-4}$ m^3/s and $\omega = 2\pi$ h^{-1}. The distance from the pumping well is 6 m to the observation well 101D and 11.5 m to well 102D. The screen lengths are 3 m from the aquifer bottom for well 101D and from the water table for well 102D. For the OPT at the Barnwell-McBean Aquifer, the formation mainly consists of

sand and fine-grained material. The pumping well has outer radius of 7.6 cm and pumping rate of $Q\sin(\omega t)$ with Q = 1.19×10^{-3} m^3/s and ω = π h^{-1}. The observation well 201C is at 6 m from the pumping well. The data of time-varying hydraulic heads at the observation wells (i.e., 101D, 102D, 201C) are plotted in Fig. 7. One can refer to Rasmussen et al. (2003) for detailed description of the Savannah River site.

The aquifer hydraulic parameters are determined based on Solutions 3 to 6 coupled with the Levenberg–Marquardt algorithm provided in the Mathematica function FindFit (Wolfram, 1991). Solutions 4 and 5 are used to predict depth-averaged head expressed as $(z'_u - z'_l)^{-1}\int_{z'_l}^{z'_u} h_s dz$ with the upper elevation z'_u and lower one z'_l of the finite screen of the observation well 101D or 102D at the Surficial Aquifer. Note that Solutions 3 and 6 are independent of elevation because of the fully-screened pumping well. Define the standard error of estimate (SEE) as $\text{SEE} = \sqrt{\frac{1}{M}\sum_{j=1}^{M} e_j^2}$ and the mean error (ME) as $\text{ME} = \frac{1}{M}\sum_{j=1}^{M} e_j$ where e_j is the difference between predicted and observed hydraulic heads and M is the number of observation data (Yeh, 1987). The estimated parameters and associated SEE and ME are displayed in Table 2. The estimates of T, S and D_r given in Rasmussen et al. (2003) are also presented. The result shows the estimated S_y is very small, and the estimated T and S by Solution 3, 6 or the Rasmussen et al. (2003) solution for confined flow are close to those by Solution 4 or 5 for unconfined flow, indicating that the unconfined flow induced by the OPT in the Surficial Aquifer is negligibly small. Little gravity drainage due to the DGD effect appears with a_1 = 20 for wells 101D and 102D as discussed in Section 3.1. Rasmussen et al. (2003) also revealed the confined behaviour of the OPT-induced flow in the Surficial Aquifer. The estimated S_y is one order less than the lower limit of the typical range of 0.01 ~ 0.3 (Freeze and Cherry, 1979), which accords with the findings of Rasmussen et al. (2003) and Rabinovich et al. (2015). Such a fact might be attributed to the problem of the moisture exchange limited by capillary fringe between the zones below and above the water table. Several laboratory

research outcomes have confirmed an estimate of S_y at short period of OPT is much smaller than that determined by constant-rate pumping test (e.g., Cartwright et al., 2003; 2005). In addition, the difference in T, S or D_r estimated by Solution 6 and those by the Rasmussen et al. (2003) solution may be attributed to the fact that their solution assumes isotropic hydraulic conductivity (i.e., $K_r = K_z$). On the other hand, transient Solution 3 gives smaller SEEs than PSS Solution 6 or the Rasmussen et al. (2003) solution for the Barnwell-McBean Aquifer and better fits to the observed data at the early pumping periods as shown in Fig. 7. From those discussed above, we may conclude the present solution is applicable to real-world OPT.

4. Concluding remarks

A variety of analytical models for OPT have been proposed so far, but little attention is paid to the joint effects of DGD, initial condition, and finite radius of a pumping well. This study develops a new model for describing hydraulic head fluctuation due to OPT in unconfined aquifers. Static hydraulic head prior to OPT is regarded as an initial condition. A Neumann boundary condition is specified at the rim of a finite-radius pumping well. A free surface equation accounting for the DGD effect is considered as the top boundary condition. The solution of the model is derived by the Laplace transform, finite-integral transform and Weber transform. The sensitivity analysis of the head response to the change in each of hydraulic parameters is performed. The observation data obtained from the OPT at the Savannah River site are analyzed by the present solution when coupling the Levenberg–Marquardt algorithm to estimate aquifer hydraulic parameters. Our findings are summarized below:

1. When $10^{-2} \leq a_1 \leq 500$, the effect of DGD on head fluctuations should be considered. The amplitude of head fluctuation predicted by DGD Solution 1 decreases with increasing a_1 to a trough and then increases to the amplitude predicted by IGD Solution 2. When $a_1 > 500$, the DGD becomes IGD. Both Solutions 1 and 2 predict the same head fluctuation. When $a_1 < 10^{-2}$ and $P < 10^4$s, the DGD results in the water table under no-flow condition. Solution 1 for unconfined flow gives an identical head prediction to

Solution 3 for confined flow.

2. Assuming a large-diameter well as a line source with infinitesimal radius underestimates the amplitude of head fluctuation in the domain of $1 \leq \bar{r} \leq 6$ when the radius exceeds 80 cm, leading to relative error RE > 10% shown in Fig. 3. In contrast, the assumption is valid in predicting the amplitude in the domain of $\bar{r} > 6$ in spite of adopting a large-diameter well. When $r_w \leq 10$ cm (i.e., RE < 0.45%), the well radius can be regarded as infinitesimal. The result is applicable to existing analytical solutions assuming infinitesimal radius and finite difference solutions treating the pumping well as a nodal point.

3. The sensitivity analysis suggests the changes in four parameters K_r, K_z, S_s and ω significantly affect head prediction in the entire aquifer domain. The change in S_y or ε causes insignificant variation in the head under water table but slight variation at the water table.

4. Analytical solutions for OPT are generally expressed as the sum of the exponential and harmonic functions of time (i.e., $\bar{h} = \bar{h}_{\exp} + \bar{A}_t \cos(\gamma t - \phi_t)$) for transient solutions (e.g., Solution 3) and harmonic function (i.e., $\bar{h}_{\mathrm{s}} = \bar{A}_s \cos(\gamma t - \phi_s)$) for PSS solutions (e.g., Solution 6). The latter assuming Eq. (17) without the initial condition produces a time shift from the SHM predicted by the $\bar{h}_{\mathrm{SHM}}$. The phase ϕ_s should be replaced by ϕ_t so that $\bar{h}_{\mathrm{s}}$ and $\bar{h}_{\mathrm{SHM}}$ are exactly the same.

References

Bakhos, T., Cardiff, M., Barrash, W., and Kitanidis, P. K.: Data processing for oscillatory pumping tests, J. Hydrol., 511, 310–319, 2014.

Black, J. H., and Kipp, K. L.: Determination of hydrogeological parameters using sinusoidal pressure tests - a theoretical appraisal, Water Resour. Res., 17(3), 686–692, 1981.

Cardiff, M., Bakhos, T., Kitanidis, P. K., and Barrash, W.: Aquifer heterogeneity

443 characterization with oscillatory pumping: Sensitivity analysis and imaging potential, Water
444 Resour. Res., 49(9), 5395–5410, 2013.
445 Cardiff, M. and Barrash, W.: 3-D transient hydraulic tomography in unconfined aquifers with
446 fast drainage response, Water Resour. Res., 47: W12518, 2011.
447 Cardiff, M. and Barrash, W.: Analytical and semi‐analytical tools for the design of oscillatory
448 pumping tests, Ground Water, 53(6), 896–907, 2014.
449 Cartwright, N., Nielsen, P., and Dunn, S.: Water table waves in an unconfined aquifer:
450 Experiments and modeling, Water Resour. Res., 39(12), 1330, 2003.
451 Cartwright, N., Nielsen, P., and Perrochet, P.: Influence of capillarity on a simple harmonic
452 oscillating water table: Sand column experiments and modeling, Water Resour. Res., 41(8),
453 W08416, 2005.
454 Christensen, N. K., Ferre, T. P. A., Fiandaca, G., and Christensen, S.: Voxel inversion of
455 airborne electromagnetic data for improved groundwater model construction and prediction
456 accuracy, Hydrol. Earth Syst. Sci., 21, 1321–1337, 2017.
457 Dagan, G. and Rabinovich, A.: Oscillatory pumping wells in phreatic, compressible, and
458 homogeneous aquifers, Water Resour. Res., 50(8), 7058–7066, 2014.
459 Fokker, P. A., Salina Borello, E., Serazio, C., and Verga, F.: Estimating reservoir
460 heterogeneities from pulse testing, J. Petrol. Sci. Eng., 86–87, 15–26, 2012.
461 Fokker, P. A., Renner, J., and Verga, F.: Numerical modeling of periodic pumping tests in
462 wells penetrating a heterogeneous aquifer, Am. J. Environ. Sci, 9(1), 1–13, 2013.
463 Freeze, R. A. and Cherry, J. A.: Groundwater, Prentice-Hall, New Jersey, 1979, 604 pp.
464 Kuo, C.: Determination of reservoir properties from sinusoidal and multirate flow tests in one
465 or more wells, SPE J., 12(6), 499–507, 1972.
466 Latinopoulos, P.: Analytical solutions for periodic well recharge in rectangular aquifers with
467 3rd-kind boundary-conditions, J. Hydrol., 77(1–4), 293–306, 1985.
468 Liang, X., Zhan, H., Zhang, Y.-K., and Liu, J.: On the coupled unsaturated-saturated flow

process induced by vertical, horizontal, and slant wells in unconfined aquifers, Hydrol. Earth Syst. Sci., 21, 1251–1262, 2017.

Liang, X., Zhan, H., Zhang, Y.-K., Liu, J.: Underdamped slug tests with unsaturated‐saturated flows by considering effects of wellbore skins, Hydrol. Process., 32, 968 – 980, 2018.

Lin, Y.-C., Yeh, H.-D.: A lagging model for describing drawdown induced by a constant-rate pumping in a leaky confined aquifer, Water Resour. Res., 53, 8500 – 8511, 2017.

Liou, T. S., and Yeh, H. D.: Conditional expectation for evaluation of risk groundwater flow and solute transport: one-dimensional analysis, J. Hydrol., 199, 378–402, 1997.

Maineult, A., Strobach, E., and Renner, J.: Self-potential signals induced by periodic pumping tests, J. Geophys. Res: Sol. Earth, 113(B1), B01203, 2008.

Moench, A. F.: Combining the Neuman and Boulton models for flow to a well in an unconfined aquifer, Ground Water, 33(3), 378–384, 1995.

Muthuwatta, L., Amarasinghe, U. A., Sood, A., and Surinaidu, L.: Reviving the "Ganges Water Machine": where and how much?, Hydrol. Earth Syst. Sci., 21, 2545–2557, 2017.

Neuman, S.P.: Theory of flow in unconfined aquifers considering delayed response of the water table, Water Resour. Res., 8(4), 1031–1045, 1972.

Povstenko, Y.: Linear fractional diffusion-wave equation for scientists and engineers. New York, Birkhäser, 2015.

Rabinovich, A., Barrash, W., Cardiff, M., Hochstetler, D., Bakhos, T., Dagan, G., and Kitanidis, P. K.: Frequency dependent hydraulic properties estimated from oscillatory pumping tests in an unconfined aquifer, J. Hydrol., 531, 2–16, 2015.

Rasmussen, T. C., Haborak, K. G., and Young, M. H.: Estimating aquifer hydraulic properties using sinusoidal pumping at the Savannah River site, South Carolina, USA, Hydrogeol. J., 11(4), 466–482, 2003.

Spane, F. A. and Mackley, R. D.: Removal of river-stage fluctuations from well response using multiple regression, Ground Water, 49(6), 794–807, 2011.

Vine, N. L., Butler, A., McIntyre, N., and Jackson, C.: Diagnosing hydrological limitations of a land surface model: application of JULES to a deep-groundwater chalk basin, Hydrol. Earth Syst. Sci., 20, 143–159, 2016.

Watlet, A., Kaufmann, O., Triantafyllou, A., Poulain, A., Chambers, J. E., Meldrum, P. I., Wilkinson, P. B., Hallet, V., Quinif, Y., Ruymbeke, M. V., and Camp, M. V.: Imageing groundwater infiltration dynamics in the karst vadose zone with long-term ERT monitoring, Hydrol. Earth Syst. Sci., 22, 1563–1592, 2018.

Wolfram, S.: Mathematica, Version 2.0. Wolfram Research, Inc., Champaign, IL, 1991.

Yeh, H. D.: Theis' solution by nonlinear least - squares and finite - difference Newton's Method, Ground Water, 25(6), 710–715, 1987.

Yeh, H. D., Chang, Y. C.: Recent advances in modeling of well hydraulics, Adv. Water Resour. 51, 27 – 51, 2013.

Yeh, T. C. J. and Liu, S. Y.: Hydraulic tomography: Development of a new aquifer test method, Water Resour. Res., 36(8), 2095–2105, 2000.

Zhou, Y. Q., Lim, D., Cupola, F., and Cardiff, M.: Aquifer imaging with pressure waves evaluation of low-impact characterization through sandbox experiments, Water Resour. Res., 52(3), 2141–2156, 2016.

Acknowledgments

Research leading to this paper has been partially supported by the grants from the Fundamental Research Funds for the Central Universities (2018B00114), the National Natural Science Foundation of China (51809080, 41561134016 and 51421006) and the Taiwan Ministry of Science and Technology under the contract numbers MOST 107-2221-E-009-019-MY3. The authors are grateful to Prof. T. C. Rasmussen for kindly providing the OPT data obtained from the Savannah River site.

519 **Table 1.** The present solution and its special cases

Well screen	Transient flow		Pseudo-steady state flow	
	Unconfined aquifer	Confined aquifer	Unconfined aquifer	Confined aquifer
Partial	Solutions 1 and 2	Solution 3	Solutions 4 and 5	Solution 6
Full	Solutions 1 and 2[a]	Solution 3[a,b]	Solutions 4 and 5[a]	Solution 6[a,b]

520 Solution 1 consists of Eqs. (14a) – (14k) with the roots of Eq. (15) and $c_0 = a_1 p_0/(p_0 + a_2)$ for DGD.

521 Solution 2 is the same as Solution 1 but has $c_0 = ap_0$ for IGD.

522 Solution 3 equals Solution 1 with Eqs. (16a) – (16d) and $\beta_n = 0,\ \pi,\ 2\pi,\ \ldots,\ n\pi$.

523 Solution 4 is the component $\bar{h}_{\mathrm{SHM}}$ of Solution 1 for DGD.

524 Solution 5 consists of Eqs. (23a) – (23m) for IGD.

525 Solution 6 consists of Eqs. (23a) – (23e) with $\bar{H}(\bar{r}, \bar{z})$ defined by Eq. (24).

526 [a] $\bar{z}_u = 1$ and $\bar{z}_l = 0$ for fully screened well

527 [b] The solution is independent of elevation.

528

Table 2. Hydraulic parameters estimated by the present solution and the Rasmussen et al. (2003) solution for OPT data from the Savannah River site

Observation well	Solution	T (m^2/s)	S	D_r (m^2/s)	K_z (m/s)	S_y	C_y (m/s)	α	κ (s)	SEE	ME
					Surficial Aquifer						
101D	Solution 3[a]	9.27×10^{-4}	2.44×10^{-3}	0.380	-	-	-	-	-	0.018	-5.56×10^{-3}
	Solution 6[b]	9.18×10^{-4}	2.33×10^{-3}	0.393	-	-	-	-	-	0.018	-2.20×10^{-4}
	Solution 4[c]	4.61×10^{-4}	3.95×10^{-3}	0.117	7.38×10^{-6}	2.23×10^{-3}	3.31×10^{-3}	0.10	94.34	0.018	-2.20×10^{-4}
	Solution 5[c]	5.25×10^{-4}	1.09×10^{-3}	0.482	2.61×10^{-5}	5.49×10^{-3}	4.75×10^{-3}	0.31	-	0.019	-2.30×10^{-4}
	Rasmussen et al. (2003)[b]	2.17×10^{-3}	1.35×10^{-4}	16.074	-	-	-	-	-	0.018	-2.20×10^{-4}
102D	Solution 3[a]	9.13×10^{-4}	1.76×10^{-3}	0.519	-	-	-	-	-	0.010	-4.38×10^{-3}
	Solution 6[b]	9.17×10^{-4}	1.67×10^{-3}	0.549	-	-	-	-	-	0.011	9.57×10^{-4}
	Solution 4[c]	9.57×10^{-5}	7.85×10^{-4}	0.122	3.68×10^{-6}	4.95×10^{-3}	7.43×10^{-4}	0.24	420.17	0.011	9.57×10^{-4}
	Solution 5[c]	9.49×10^{-5}	3.25×10^{-4}	0.292	4.67×10^{-6}	4.68×10^{-3}	9.98×10^{-4}	0.31	-	0.011	9.50×10^{-4}
	Rasmussen et al. (2003)[b]	2.27×10^{-3}	2.28×10^{-4}	9.956	-	-	-	-	-	0.011	9.57×10^{-4}
					Barnwell-McBean Aquifer						
201C	Solution 3[a]	5.86×10^{-5}	7.07×10^{-4}	0.083	-	-	-	-	-	0.232	0.046
	Solution 6[b]	6.03×10^{-5}	6.54×10^{-4}	0.092	-	-	-	-	-	0.363	0.281
	Rasmussen et al. (2003)[b]	6.90×10^{-5}	4.74×10^{-4}	0.150	-	-	-	-	-	0.363	0.281

[a] transient confined flow

[b] PSS confined flow

[c] PSS unconfined flow

Figures

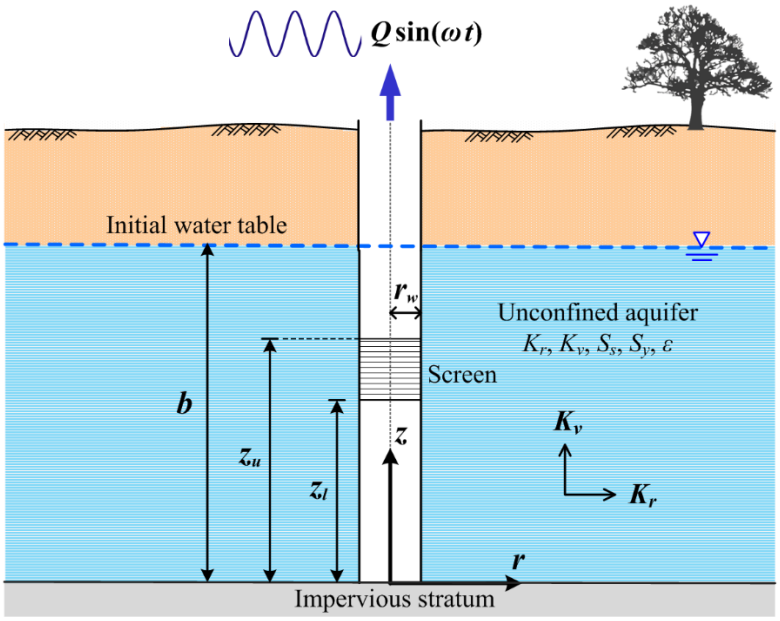

Figure 1. Schematic diagram for oscillatory pumping test at a partially screened well of finite radius in an unconfined aquifer.

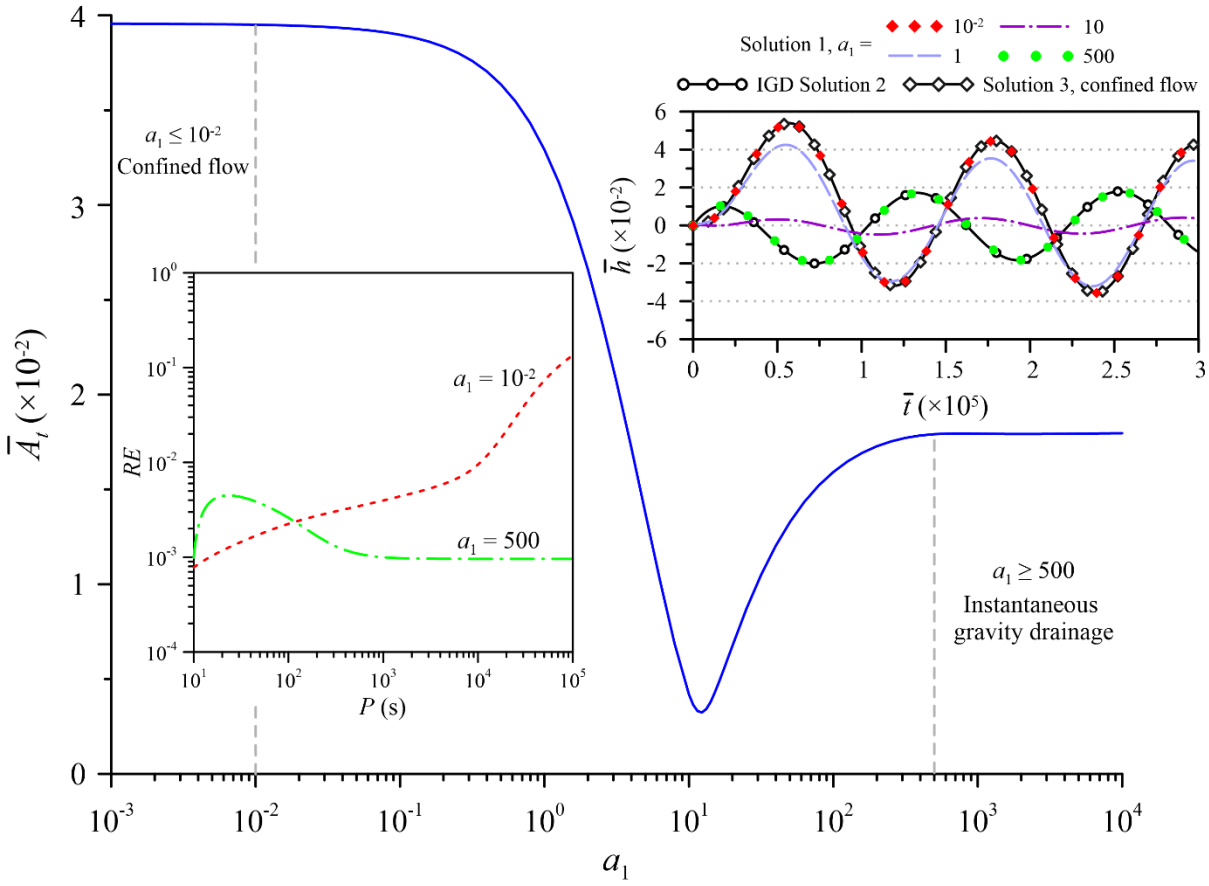

Figure 2. Influence of delayed gravity drainage on the dimensionless amplitude $\bar{A}_t$ and transient head $\bar{h}$ at $\bar{r} = 1$, $\bar{z} = 1$ predicted by Solution 1 for different magnitudes of a_1 related to the influence.

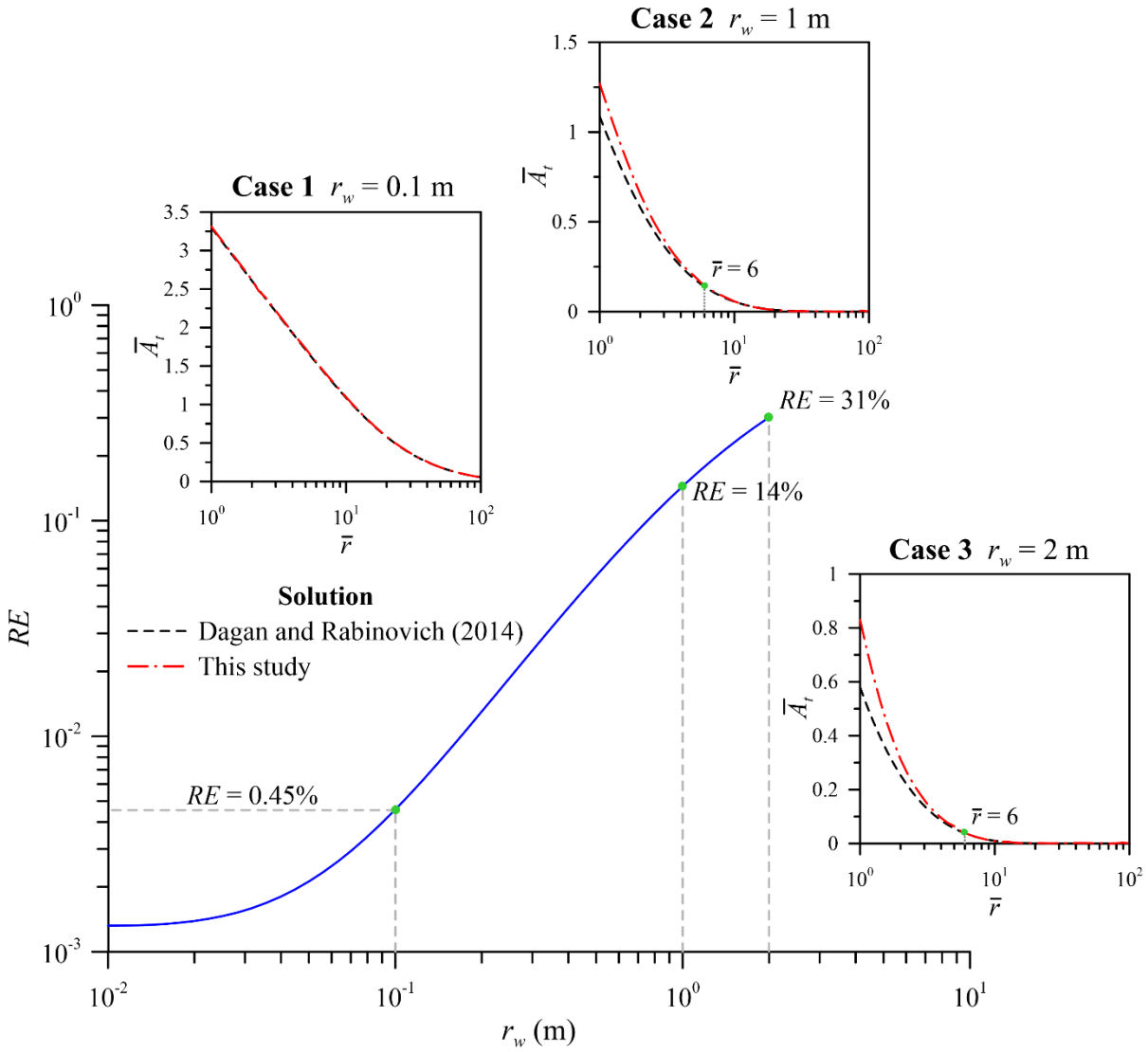

542

543 **Figure 3.** Relative error (*RE*) on the dimensionless amplitudes $\bar{A}_t$ at the rim of the pumping
544 well (i.e., $r = r_w$) predicted by IGD Solution 2 and the Dagan and Rabinovich (2014) solution.
545 The well radius is assumed infinitesimal in the Dagan and Rabinovich (2014) solution and
546 finite in our solution.

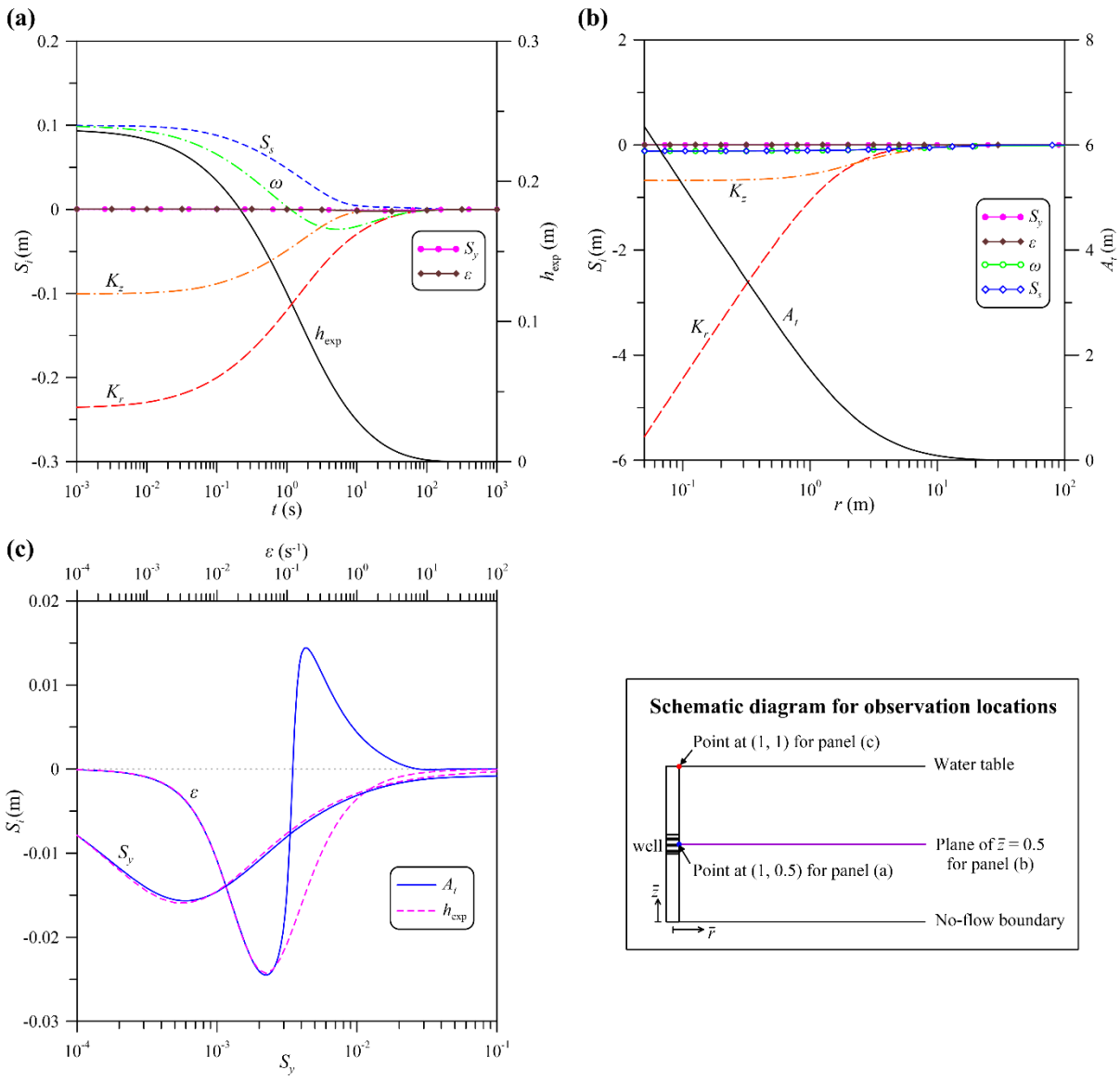

Figure 4. The normalized sensitivity coefficient S_i associated with (a) the exponential component h_{exp} of Solution 1 and (b) the SHM amplitude A_t for parameters K_r, K_z, S_s, S_y, ω and ε. The observation locations for panels (a) and (b) are under water table (i.e., $\bar{z} = 0.5$). Panel (c) displays the curves of S_i of h_{exp} and A_t at water table (i.e., $\bar{z} = 1$) versus S_y and ε.

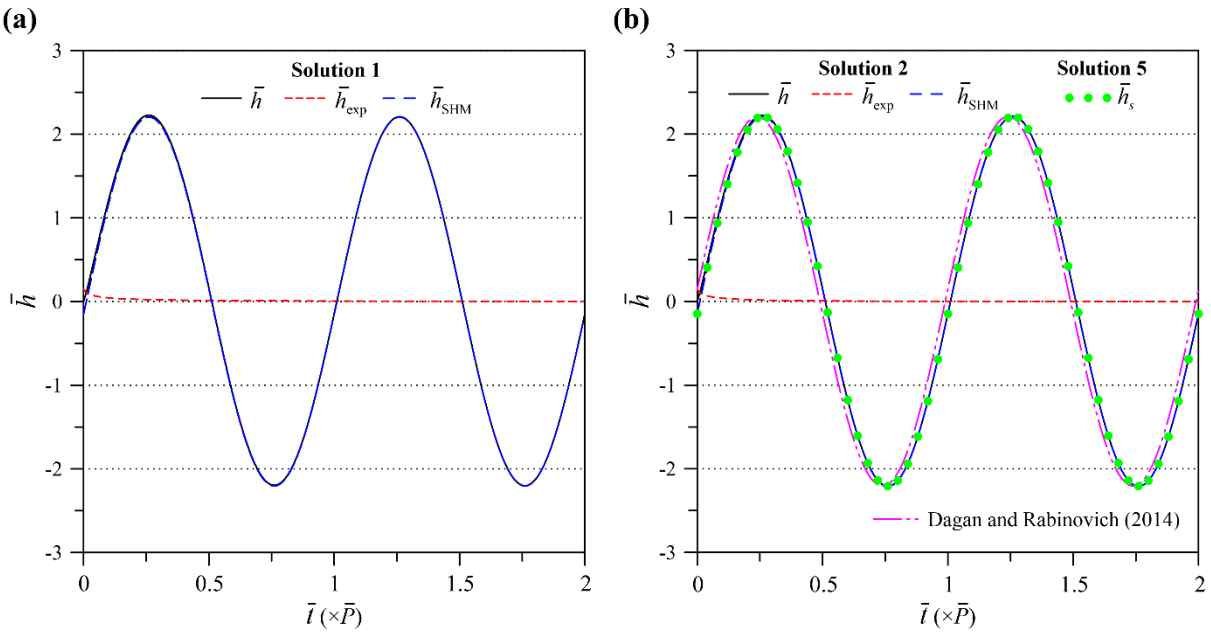

553

554 **Figure 5.** Heads fluctuations at $\bar{r} = 6$ predicted by (a) DGD Solution 1 and (b) IGD Solution
555 2. Solutions 1 and 2 are expressed as $\bar{h} = \bar{h}_{\text{exp}} + \bar{h}_{\text{SHM}}$ for transient flow. IGD Solution 5
556 expressed as $\bar{h}_s = \bar{A}_s \cos(\gamma t - \phi_s)$ accounts for PSS flow.

557

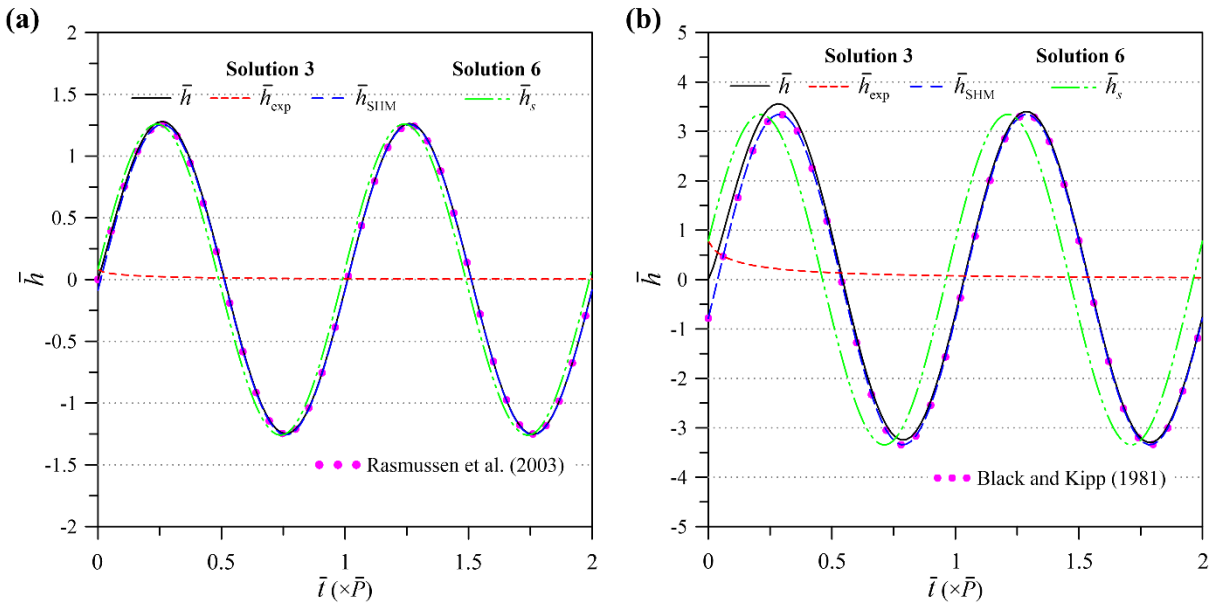

558

559 **Figure 6.** Heads fluctuations at $\bar{r} = 6$ predicted by Solutions 3 and 6 for (a) partially-screened

560 pumping well and (b) fully-screened pumping well. Solution 3 is expressed as $\bar{h} = \bar{h}_{\text{exp}} +$

561 $\bar{h}_{\text{SHM}}$ for transient flow. Solution 6 expressed as $\bar{h}_s = \bar{A}_s \cos(\gamma t - \phi_s)$ accounts for PSS

562 flow.

563

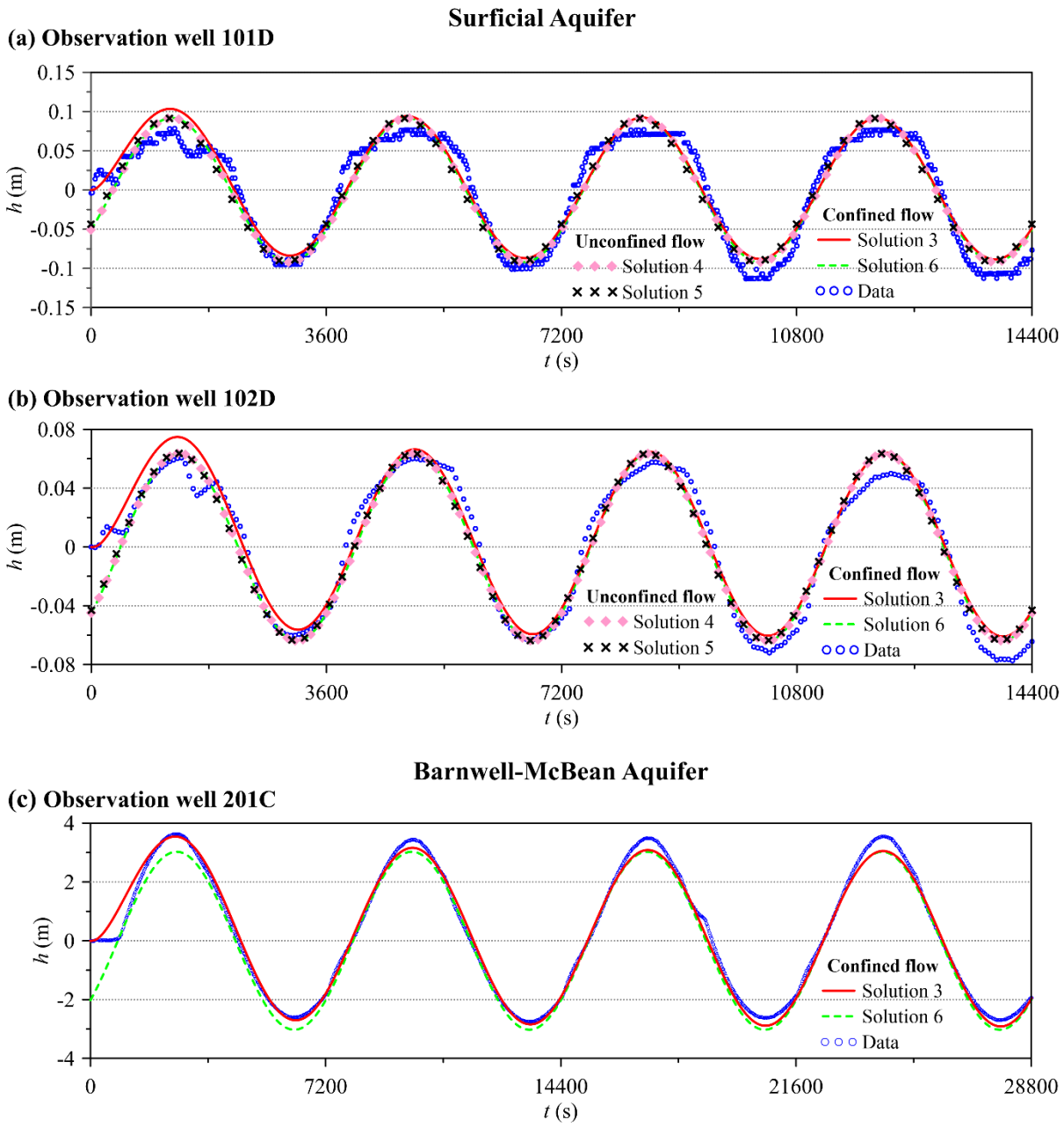

564

565 **Figure 7.** Comparision of field observation data with head fluctuations predicted by the present
566 solution. Solutions 3 and 6 represent transient and PSS confined flows, respectively. PSS
567 Solutions 4 and 5 stand for DGD and IGD conditions, respectively.

568